CLOSED-FORM DETECTOR FOR SOLID SUB-PIXEL TARGETS IN MULTIVARIATE T-DISTRIBUTED BACKGROUND CLUTTER

James Theiler[a], Beate Zimmer[b], and Amanda Ziemann[a]

[a]Space Data Science and Systems Group, Los Alamos National Laboratory, Los Alamos, NM
[b]Department of Mathematics and Statistics, Texas A&M University–Corpus Christi, Corpus Christi, TX

ABSTRACT

The generalized likelihood ratio test (GLRT) is used to derive a detector for solid sub-pixel targets in hyperspectral imagery. A closed-form solution is obtained that optimizes the replacement target model when the background is a fat-tailed elliptically-contoured multivariate t-distribution. This generalizes GLRT-based detectors that have previously been derived for the replacement target model with Gaussian background, and for the additive target model with an elliptically-contoured background. Experiments with simulated hyperspectral data illustrate the performance of this detector in various parameter regimes.

Index Terms— Adaptive signal detection, algorithms, data models, detectors, multidimensional signal processing, pattern recognition, remote sensing, spectral image analysis.

1. INTRODUCTION

To detect small targets in cluttered backgrounds requires models of the target, of the background, and of how the two interact. Although target variability models are important, particularly for solid targets [1], we will take the target signature as a single vector. However, we will consider a range of elliptically-contoured background models, from Gaussian to very fat tailed, and we will consider two different target-background interaction models – the additive model and the replacement model – that incorporate variability into the *strength* of the target.

1.1. Background models

The importance of background modeling has recently been emphasized [2], and although the Gaussian model is often surprisingly effective, a useful extension is the multivariate t-distribution, which has in particular been proposed for hyperspectral imagery [3]. This is similar to the Gaussian in that it is defined by a mean and a covariance matrix, which implies that the distribution is uni-modal with ellipsoidal contours of

constant density; this density decreases with distance from the mean, but the decrease can be much slower than the $\exp(-r^2)$ decay exhibited by Gaussians, leading to heavier tails that are often more representative of observed data.

1.2. Target-background interaction models

In many signal detection applications, the signal of interest is assumed to be additive with respect to a background that is generally characterized in some statistical way. We can write

$$\mathbf{x} = \mathbf{z} + \alpha\mathbf{t} \tag{1}$$

where $\mathbf{x} \in \mathbb{R}^d$ is the measured signal, $\mathbf{z} \in \mathbb{R}^d$ is the background signal, $\mathbf{t} \in \mathbb{R}^d$ is the signal of interest, d is the number of spectral channels, and α is a scalar quantity that characterizes the strength of the signal. The additive model is the basis for many traditional target detection algorithms, including the adaptive matched filter (AMF) [4] and the adaptive coherence estimator (ACE) [5]. When the background is multivariate t, then the GLRT solution for the additive model leads to a detector we will here call the elliptically-contoured adaptive matched filter[1] (EC-AMF) [6]; it is given by

$$\mathcal{D}(\mathbf{x}) = \frac{\sqrt{(\nu - 1)}\ \mathbf{t}^{\mathsf{T}} R^{-1}(\mathbf{x} - \boldsymbol{\mu})}{\sqrt{(\nu - 2) + (\mathbf{x} - \boldsymbol{\mu})^{\mathsf{T}} R^{-1}(\mathbf{x} - \boldsymbol{\mu})}}, \tag{2}$$

where $\boldsymbol{\mu}$ is the mean and R is the covariance matrix of the background distribution. In Eq. (2), $\nu \to \infty$ leads to the AMF detector, and $\nu \to 2$ leads to the ACE detector.

While the additive model is the basis for many target detection algorithms, it has limitations [7], and in particular does not account for the occlusion of the background by a solid target. In the replacement model [8, 9], we treat $0 \leq \alpha \leq 1$ as the target area (fraction of a pixel), and write

$$\mathbf{x} = (1 - \alpha)\mathbf{z} + \alpha\mathbf{t}. \tag{3}$$

This is called the replacement model because a fraction α of the background signal $\mathbf{z}$ is *replaced* with target signal $\mathbf{t}$. The

---

[1]In [6], it is given a different name (EC-GLRT) that is not as consistent with the naming conventions used in this paper.

---

finite target matched filter (FTMF), derived by Schaum and Stocker [10], is the replacement-model version of the AMF: it is the GLRT solution to Eq. (3) in the situation that the background $\mathbf{z}$ is Gaussian. Although this detector is somewhat more complicated than the AMF, or even the EC-AMF in Eq. (2), it can be written as a closed-form expression.

Closed-form generalizations of the FTMF have been derived for Gaussian target variability [11] and alternative models of covariance scaling [12]. Here, we derive a closed-form GLRT solution when the background is a general class of elliptically-contoured distribution. In the special case that the background is Gaussian, we obtain the FTMF solution.

We treat the target detection problem in a hypothesis testing framework, with the null hypothesis corresponding to $\alpha = 0$ and the alternative associated with $\alpha > 0$. Since the nonzero α is unspecified, this is a composite hypothesis testing problem [13], and we use the generalized likelihood ratio test (GLRT) to derive our detector. The detector is a function of $\mathbf{x}$ given by the logarithm of this ratio

$$\mathcal{D}(\mathbf{x}) = \log \frac{\max_\alpha p_x(\mathbf{x}|\alpha)}{p_x(\mathbf{x}|0)}. \qquad (4)$$

The expression in Eq. (4) is written in terms of p_x, which is the probability density function for $\mathbf{x}$. We can express this function in terms of $p_z(\mathbf{z})$, the probability density associated with the background $\mathbf{z}$. We have

$$p_x(\mathbf{x}|\alpha) = (1-\alpha)^{-d} p_z((\mathbf{x} - \alpha\mathbf{t})/(1-\alpha)) \qquad (5)$$

where the argument $(\mathbf{x} - \alpha\mathbf{t})/(1-\alpha)$ is obtained by solving Eq. (3) for $\mathbf{z}$, and where the prefactor $(1-\alpha)^{-d}$ arises from the Jacobian of the transformation of variables from p_x to p_z.

Taking $\mathbf{z}$ to have mean $\boldsymbol{\mu}$ and covariance R, the multivariate t distribution is given by

$$p_z(\mathbf{z}) = c\,|R|^{-d/2}\left(1 + \frac{(\mathbf{z} - \boldsymbol{\mu})^\mathsf{T} R^{-1}(\mathbf{z} - \boldsymbol{\mu})}{\nu - 2}\right)^{-\frac{d+\nu}{2}} \qquad (6)$$

where d is number of spectral channels, ν is a parameter that specifies how fat-tailed the distribution is (larger ν is less fat-tailed, with the $\nu \to \infty$ limit corresponding to a Gaussian distribution), and the normalizing constant c depends only on d and ν. Thus,

$$p_x(\mathbf{x}|\alpha) = (1-\alpha)^{-d} p_z((\mathbf{x} - \alpha\mathbf{t})/(1-\alpha)) \qquad (7)$$

$$= \frac{c\,|R|^{-d/2}}{(1-\alpha)^d}\left(1 + \frac{\mathbf{w}^\mathsf{T} R^{-1}\mathbf{w}}{(1-\alpha)^2(\nu - 2)}\right)^{-\frac{d+\nu}{2}} \qquad (8)$$

where $\mathbf{w} = (\mathbf{x} - \mu) - \alpha(\mathbf{t} - \mu)$. To find the value of α that maximizes Eq. (8), we can take the derivative of $\log p(\mathbf{x}|\alpha)$ with respect to α, set that expression to zero, and solve for α. For Gaussian $p_z(\mathbf{z})$, that approach was found [10] to produce a quadratic equation in α. For the more general multivariate t-distribution, we also obtain a quadratic equation, though with

Table 1. Taxonomy of detection algorithms. The EC-FTMF (and its special case FTCE) are introduced in this paper, to extend the FTMF algorithm to non-Gaussian backgrounds.

Target model	Gaussian $\nu \to \infty$	Multivariate t $2 \le \nu \le \infty$	Fat-tailed $\nu \to 2$
Additive	AMF [4]	EC-AMF [6]	ACE [5]
Replacement	FTMF [10]	EC-FTMF	FTCE

modified coefficients. The solution to that quadratic equation is given by

$$\widehat{\alpha} = 1 - \frac{-B + \sqrt{B^2 - 4AC}}{2A} \qquad (9)$$

where

$$A = (\mathbf{t} - \boldsymbol{\mu})^\mathsf{T} R^{-1}(\mathbf{t} - \boldsymbol{\mu}) + (\nu - 2), \qquad (10)$$

$$B = (1 - \nu/d)(\mathbf{x} - \mathbf{t})^\mathsf{T} R^{-1}(\mathbf{t} - \boldsymbol{\mu}), \qquad (11)$$

$$C = -(\nu/d)(\mathbf{x} - \mathbf{t})^\mathsf{T} R^{-1}(\mathbf{x} - \mathbf{t}). \qquad (12)$$

This value of α satisfies $p_x(\mathbf{x}|\widehat{\alpha}) = \max_\alpha p_x(\mathbf{x}|\alpha)$. Thus, our detector, the elliptically-contoured finite target matched filter (EC-FTMF), is given by

$$\mathcal{D}(\mathbf{x}) = \log p_x(\mathbf{x}|\widehat{\alpha}) - \log p_x(\mathbf{x}|0) \qquad (13)$$

with $p_x(\mathbf{x}|\alpha)$ given in Eq. (8) and $\widehat{\alpha}$ given by Eqs. (9-12).

In the $\nu \to \infty$ limit, the multivariate t becomes Gaussian, and the expressions in Eqs. (10-12) diverge. But in Eq. (9) it is only the relative values that matter; thus we can express this limit with the expressions

$$B/A = -(\mathbf{x} - \mathbf{t})^\mathsf{T} R^{-1}(\mathbf{t} - \boldsymbol{\mu})/d, \qquad (14)$$

$$C/A = -(\mathbf{x} - \mathbf{t})^\mathsf{T} R^{-1}(\mathbf{x} - \mathbf{t})/d. \qquad (15)$$

These values recapitulate the FTMF result obtained for a Gaussian background [10].

For $\nu \to 2$, we have the heavy-tailed limit

$$A = (\mathbf{t} - \boldsymbol{\mu})^\mathsf{T} R^{-1}(\mathbf{t} - \boldsymbol{\mu}), \qquad (16)$$

$$B = (1 - 2/d)(\mathbf{x} - \mathbf{t})^\mathsf{T} R^{-1}(\mathbf{t} - \boldsymbol{\mu}), \qquad (17)$$

$$C = -(2/d)(\mathbf{x} - \mathbf{t})^\mathsf{T} R^{-1}(\mathbf{x} - \mathbf{t}), \qquad (18)$$

which we call the finite target coherence estimator (FTCE).

We remark that these three replacement-model detectors, the general EC-FTMF and the special cases FTMF and FTCE, have corresponding detectors associated with the additive model in Eq. (1), as shown in Table 1. These additive-model detectors are the EC-AMF and its special cases, AMF and ACE. For very small α and very large target magnitude $|\mathbf{t}|$, we expect these replacement-model detectors to be well approximated by their associated additive-model detectors. In this sense, we can argue that the EC-FTMF detector described in Eq. (13) covers all six cases.
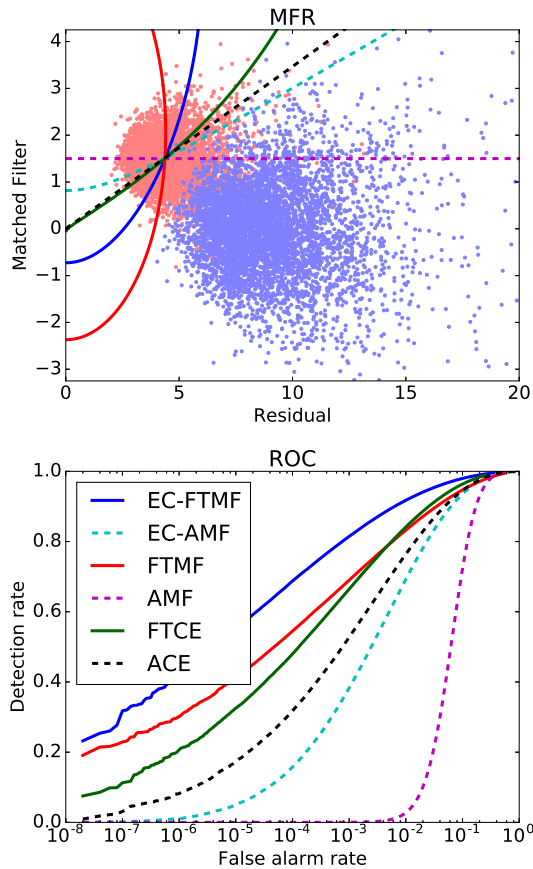
Fig. 1. Top panel is Matched-Filter Residual (MFR) plot of simulated data, showing both background (blue) and target (red) pixels, along with the contours associated with several different detection algorithms. The contours are chosen so that the detection rate is exactly 0.5; the better detectors are those with fewer false alarms, which are associated with blue pixels that are "above" the contours. Bottom panel is Receiver Operating Characteristic (ROC) curves for these detectors. Here, $\nu = 10$, $d = 90$, $T = 3$, and $\alpha = 0.5$.

2. SIMULATION

We can illustrate the performance of the EC-FTMF detector on simulated data. In this simulation we draw N samples from a d-dimensional multivariate t-distribution parameterized by ν, with (for simplicity) zero mean and unit covariance. These N samples are representative of background pixels from a multi- or hyper-spectral image that have been de-meaned and whitened.

For each background sample, we used the matched-pair formulation [14, 15] to produce an associated target pixel, produced by the replacement model in Eq. (3) using a fixed value of α (which we know, but the algorithm does not). Our target signature $\mathbf{t}$ is given by a vector of magnitude T.

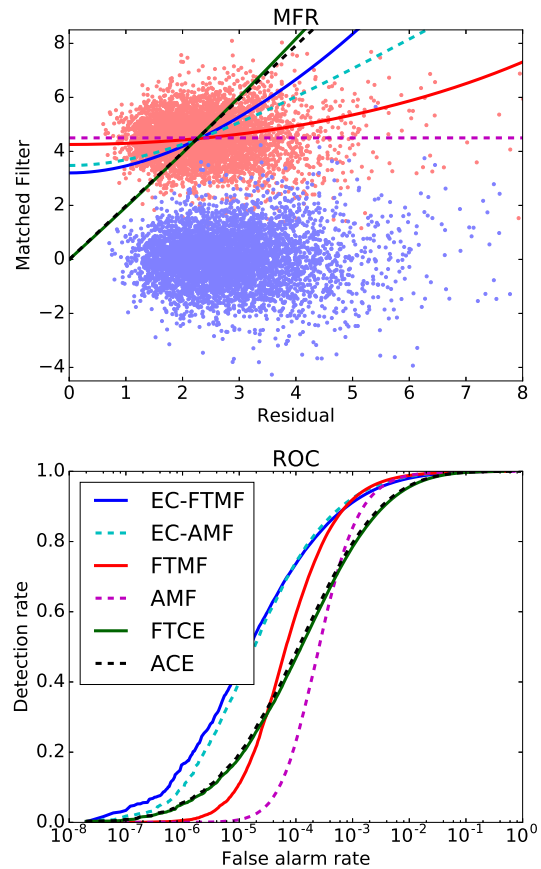The background and target pixels are d-dimensional

Fig. 2. Here, $\nu = 10$, $d = 10$, $T = 30$, and $\alpha = 0.15$. The target is strong ($T \gg 1$) and small ($\alpha \ll 1$), so the effect due to occlusion is limited, but still discernible. Here, the additive-model detectors do almost (but not quite) as well as the corresponding replacement-model detectors.

vectors $\mathbf{x}$, but are presented in a two-dimensional matched-filter-residual (MFR) plot [16] in which the matched-filter magnitude MF is plotted on the y-axis and the residual R is on the x-axis. In this zero-mean unit-covariance case:

$$\text{MF} = \mathbf{t}^\mathsf{T}\mathbf{x}/T \tag{19}$$

$$\text{R} = \sqrt{\mathbf{x}^\mathsf{T}\mathbf{x} - (\text{MF})^2}. \tag{20}$$

Fig. 1 illustrates these pixels as points in a scatter-plot. The reason for choosing this representation is that all of the detectors we consider here have contours that can be plotted in this two-dimensional space. Fig. 1 also compares the performance of various detectors on this simulated data, and for these parameters, we see that the new EC-FTMF detector does well. The original FTMF is confounded because it incorrectly assumes the background is Gaussian; the ACE, AMF, and EC-AMF detectors are confounded because they incorrectly assume the additive target model.

In the regime of very large T and very small α, the

replacement model is "nearly" additive. In Fig. 2, we observe that the replacement-model and additive-model variants of the same detectors are similar, although EC-FTMF is still discernibly better than EC-AMF, and FTMF is substantially better than AMF. Interestingly, FTCE is no better than ACE.

We have observed (results not shown here) that larger T and smaller α lead to a regime in which replacement-model and additive-model variants are virtually identical.

3. DISCUSSION

In introducing the EC-FTMF detector, and showing that the GLRT solution can be expressed in closed form, we obtain a target detection algorithm that is both convenient and adaptive to a range of conditions. In practice, using EC-FTMF (just as in using EC-AMF or other EC-based algorithms), one must estimate the multivariate t-distribution parameter ν that describes the fatness of the tails. To keep things simple, our simulations employed the same ν in the algorithm that was used for the simulation. But estimation of the single scalar parameter ν from a large dataset is not that difficult; one simple approach employs higher moments of the whitened data [17].

Finally, we remark that the GLRT – although widely used, and very often with good results – is not the only or necessarily the optimal solution to the composite hypothesis testing problem. One may prefer Bayesian approaches [13] or the recently introduced clairvoyant fusion [18, 19].

4. REFERENCES

[1] T. L. Myers, C. S. Brauer, Y.-F. Su, T. A. Blake, R. G. Tonkyn, A. B. Ertel, T. J. Johnson, and R. L. Richardson, "Quantitative reflectance spectra of solid powders as a function of particle size," *Applied Optics*, vol. 54, pp. 4863–4875, 2015.

[2] S. Matteoli, M. Diani, and J. Theiler, "An overview background modeling for detection of targets and anomalies in hyperspectral remotely sensed imagery," *IEEE J. Sel. Topics in Applied Earth Observations and Remote Sensing*, vol. 7, pp. 2317–2336, 2014.

[3] D. Manolakis, D. Marden, J. Kerekes, and G. Shaw, "On the statistics of hyperspectral imaging data," *Proc. SPIE*, vol. 4381, pp. 308–316, 2001.

[4] I. S. Reed, J. D. Mallett, and L. E. Brennan, "Rapid convergence rate in adaptive arrays," *IEEE Trans. Aerospace and Electronic Systems*, vol. 10, pp. 853–863, 1974.

[5] S. Kraut, L. L. Scharf, and R. W. Butler, "The Adaptive Coherence Estimator: a uniformly most-powerful-invariant adaptive detection statistic," *IEEE Trans. Signal Processing*, vol. 53, pp. 427–438, 2005.

[6] J. Theiler and B. R. Foy, "EC-GLRT: Detecting weak plumes in non-Gaussian hyperspectral clutter using an elliptically-contoured generalized likelihood ratio test," *Proc. IEEE International Geoscience and Remote Sensing Symposium (IGARSS)*, p. I:221, 2008.

[7] A. Schaum, "Enough with the additive target model," *Proc. SPIE*, vol. 9088, p. 90880C, 2014.

[8] A. D. Stocker and A. P. Schaum, "Application of stochastic mixing models to hyperspectral detection problems," *Proc. SPIE*, vol. 3071, pp. 47–60, 1997.

[9] D. Manolakis, C. Siracusa, and G. Shaw, "Hyperspectral subpixel target detection using the linear mixing model," *Trans. Geoscience and Remote Sensing*, vol. 39, pp. 1392–1409, 2001.

[10] A. Schaum and A. Stocker, "Spectrally selective target detection," *Proc. ISSSR (International Symposium on Spectral Sensing Research)*, p. 23, 1997.

[11] R. S. DiPietro, D. G. Manolakis, R. B. Lockwood, T. Cooley, and J. Jacobson, "Performance evaluation of hyperspectral detection algorithms for sub-pixel objects," *Proc. SPIE*, vol. 7695, p. 76951W, 2010.

[12] A. Schaum, "Continuum fusion solutions for replacement target models in electro-optic detection," *Applied Optics*, vol. 53, pp. C25–C31, 2014.

[13] E. L. Lehmann and J. P. Romano, *Testing Statistical Hypotheses*. New York: Springer, 2005.

[14] J. Theiler, "Matched-pair machine learning," *Technometrics*, vol. 55, pp. 536–547, 2013.

[15] ——, "Transductive and matched-pair machine learning for difficult target detection problems," *Proc. SPIE*, vol. 9088, p. 90880E, 2014.

[16] B. R. Foy, J. Theiler, and A. M. Fraser, "Decision boundaries in two dimensions for target detection in hyperspectral imagery," *Optics Express*, vol. 17, pp. 17 391–17 411, 2009.

[17] J. Theiler, C. Scovel, B. Wohlberg, and B. R. Foy, "Elliptically-contoured distributions for anomalous change detection in hyperspectral imagery," *IEEE Geoscience and Remote Sensing Lett.*, vol. 7, pp. 271–275, 2010, the moment method for estimating ν is described in the Appendix.

[18] A. Schaum, "Continuum fusion: a theory of inference, with applications to hyperspectral detection," *Optics Express*, vol. 18, pp. 8171–8181, 2010.

[19] J. Theiler, "Confusion and clairvoyance: some remarks on the composite hypothesis testing problem," *Proc. SPIE*, vol. 8390, p. 839003, 2012.